Journal of Innovation and Development
ISSN: 2958-4752 | Vol. 10, No. 2, 2025

Pore Structure Characteristics of the Jurassic Dongyuemiao Shale Reservoir in the Fuxing Area, Sichuan Basin

Xuan Du[1, 2]

[1]School of Earth Sciences and Engineering, Xi'an Shiyou University, Xi'an 710065, China
[2]Shanxi Key Laboratory of Oil and Gas Accumulation Geology, Xi'an Shiyou University, Xi'an 710065, China

Abstract: XRD analysis reveals that the shale mineral composition in the study area is dominated by clay minerals (15.21%–79.68%, avg. 59.88%), primarily illite, with subordinate chlorite and kaolinite, followed by quartz (10.24%–45.84%, avg. 21.59%). Total organic carbon (TOC) ranges from 0.391% to 2.19%, with kerogen types predominantly sapropelic-humic (Type II_2) and humic (Type III). Vitrinite reflectance (R_o = 1.52%–1.54%) indicates high thermal maturity. Pore systems are dominated by parallel-plate interlayer clay pores, supplemented by calcite intraparticle pores, interparticle pores, and organic-hosted pores. Based on pore size classification, mesopores (2–50 nm) contribute the largest proportion to total pore volume, followed by macropores (>50 nm) and micropores (<2 nm). The influence of mineralogy and TOC on pore structure varies by lithofacies: in clay-rich shales, clay minerals and TOC synergistically enhance pore development, while in silty shales, quartz content exhibits a positive correlation with pore volume, likely due to grain-supported frameworks preserving primary porosity.

Keywords: Pore structure; shale reservoir; Jurassic; Sichuan Basin.

1. Introduction

In recent years, continuous exploration of shale gas has led to significant increases in reserves and production, continuously optimizing the domestic energy structure and making substantial contributions to energy security [1,3]. Since the commercial development of shale gas in the Wufeng–Longmaxi formations was achieved by Well Jiaoye 1HF in 2012, China has successively discovered marine shale gas fields such as Fuling, Changning, Zhaotong, Weiyuan, Weirong, and Yongchuan [4]. The first risk well specifically targeting terrestrial shale gas in the Dongyuemiao Member, Well Fuye 10 in the Fuxing area, was deployed in September 2018, with drilling completion in early 2019 [1,5,6]. In recent years, China Petroleum & Chemical Corporation (Sinopec) and China National Petroleum Corporation (CNPC) have focused on the exploration and development of Jurassic terrestrial shale oil and gas, as well as tight oil and gas in the Sichuan Basin, achieving some progress [7]. However, the exploration and development efforts in the Fuxing area of the Sichuan Basin remain relatively limited, and research on the Dongyuemiao Member reservoir is even scarcer. This study focuses on the shale reservoir of the Dongyuemiao Member to investigate the influencing factors of pore structure in shale.

2. Regional Geological Setting

The Sichuan Basin, covering an area of approximately 260,000 km², is one of China's most significant basins. It is characterized by fertile land and abundant oil and gas resources, as well as mineral deposits [8]. During the early Middle Jurassic, the Sichuan Basin formed as a large intracratonic sag basin due to extensional tectonics in the Upper Yangtze region. The study area is situated in the eastern Sichuan Basin, primarily within the Liangping, Dianjiang, and Fengdu districts of Chongqing. Structurally, it belongs to the Wanxian Syncline within the eastern Sichuan high-steep fault-fold belt, featuring multiple synclines developed from northwest to southeast [9,10]. Following these stages, the basin underwent structural modifications during the Himalayan orogeny, ultimately forming its current configuration [11]. Vertically, the eastern Sichuan region exhibits structural and evolutionary heterogeneity. Multi-phase tectonic activities, coupled with the interplay of multiple detachment layers, have resulted in a complex alternating pattern of anticlines and synclines, forming an alternating fold structure [12].

3. Reservoir Characteristics

3.1. Mineral Composition

Based on XRD analysis results, the shale mineral composition of the Dongyuemiao Member in the study area is predominantly clay minerals, followed by quartz, calcite, and albite, with minor amounts of pyrite, ferroan dolomite, and halite. The Dongyuemiao Member exhibits approximately 60% clay mineral content, 20% quartz, and 17% calcite (Figure 1).

The Dongyuemiao Member is subdivided into three sub-members: D1, D2, and D3, which are further divided into seven sub-layers. Sub-layers 6 and 7 belong to the D3 sub-member, sub-layer 5 to the D2 sub-member, and sub-layers 1-4 to the D1 sub-member.

In the D3 sub-member, clay minerals constitute the highest content (62.69%), followed by quartz (27.72%), with calcite being the lowest (4.89%). The D2 sub-member exhibits the highest calcite content (50.54%), followed by clay minerals (27.36%), and the lowest quartz content (20.92%). The D1 sub-member is dominated by clay minerals (69.44%), with quartz as the secondary component (18.37%) and calcite as the least abundant (10.85%).

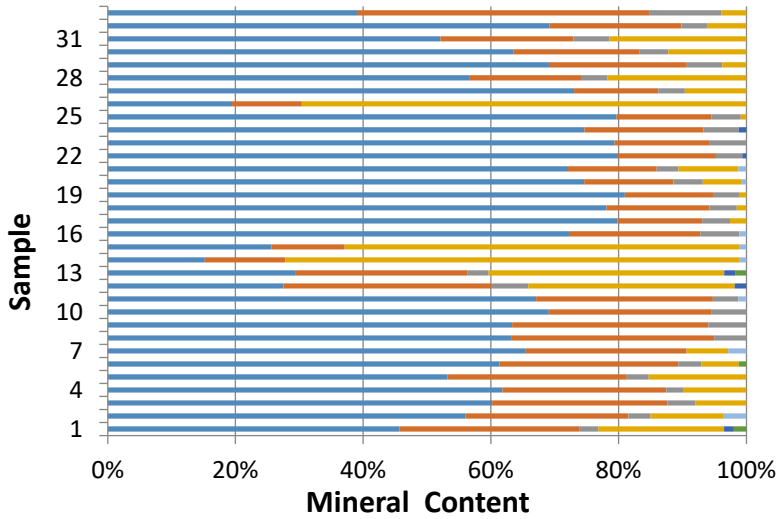


Figure 1. Bar Chart of Mineral Composition in the Dongyuemiao Member Shale Reservoir

Table 1. Mineral Composition of Shale Samples from Sub-layers in Well FY10

Sub-member		D3		D2	D1			
Sub-layer		7	6	5	4	3	2	1
Depth (m)		2752.31-2768.2	2770.89-2775.31	2778.11-2782.5	2784.8-2788.98	2791.45-2796.01	2797.65-2804.21	2806.65-2812.01
Mineral Content (%)	Illite	26.89-38.52 /34.58	33.88-39.14 /37.03	8.03-18.74 /13.74	46.8-56.52 /53.15	45.96-53.32 /49.92	8.19-54.78 /36.37	26.6-41 /31.55
	Chlorite	9.58-14.54 /12.75	15.18-22.47 /19.45	4.78-6.95 /5.86	15.83-27.2 /20.83	15.02-26.58 /22.06	10.03-32.68 /19.51	12.87-22.93 /18.03
	Kaolinite	7.4-22.51 /12.38	7.45-10.71 /9.21	6.08-9.09 /7.76	2.76-8.59 /5.28	7.9-10.07 /8.98	3.95-7.21 /5.71	4.97-7.63 /6.35
	Quartz	24.2-28.2 /26.55	25.5-31.68 /28.89	11.44-32.61/20.92	13.23-20.54 /15.52	13.9-18.69 /15.71	10.24-21.58 /15.48	19.81-45.84 /26.79
	Albite	2.75-4.4 /3.43	3.99-5.94 /5.10	3.27-5.71 /4.49	4.06-6.13 /4.69	3.4-5.73 /4.68（4）	4.1-5.55 /4.60	4.05-11.17 /6.31
	Calcite	1.71-19.69 /9.78		32.3-61.86 /50.54	1.16-6 /2.80	9.39-9.39 /9.39	0.89-65.18 /20.25	3.95-21.46 /10.95
	Pyrite	1.53-1.53 /1.53		1.7-1.85 /1.775		0.64-1.21 /0.925		
	Ferroan Dolomite	1.19-1.96 /1.575		1.77-1.77 /1.77				
	Halite	2.85-3.54 /3.195	1.26-1.26 /1.26	1.03-1.03 /1.03	0.83-1.11 /0.97	1.25-1.25 /1.25		

Format Specifications: Min–Max/Mean

This study adopts the lithofacies classification scheme proposed by Liu Zhongbao et al. [13], using a ternary diagram method with three end members (carbonate minerals, felsic minerals, and clay minerals) for rock nomenclature zoning. A 50% threshold defines dominant lithologies, dividing the ternary diagram into three end-member zones: mudstone/shale lithofacies zone, siltstone lithofacies zone, and limestone/dolostone lithofacies zone, with intermediate zones classified as mixed lithofacies.

The Dongyuemiao Member shale develops seven lithofacies: clay-rich shale facies (I_1), silty shale facies (I_3), clay-silt mixed shale facies (II_2), calcareous-silty shale facies (II_3), limestone/dolostone facies (III_1), argillaceous limestone/dolostone facies (III_2), and muddy siltstone facies (IV_2). Among these, clay-rich shale facies (I_1) and silty shale facies (I_3) are the dominant types.

The D3 sub-member primarily develops silty shale facies (I_3), the D2 sub-member mainly contains limestone facies (III_1) and argillaceous limestone facies (III_2), while the D1 sub-member is dominated by clay-rich shale facies (I_1).

A total of 33 samples were analyzed, with clay-rich shale and silty shale being most abundant.

Table 2. Shale Lithofacies Statistics

sub-member	Sub-layer	Depth (m)	Samples (count)	Lithofacies Type & Count			
				Clay shale	Silty shale	Siltstone	Limestone
D3	7	2752.31-2768.2	7	2	5		
	6	2770.89-2775.31	4		4		
D2	5	2778.11-2782.5	4		1	1	2
D1	4	2784.8-2788.98	5	4	1		
	3	2791.45-2796.01	4	4			
	2	2797.65-2804.21	5	3	2		
	1	2806.65-2812.01	4	1	2	1	

4. Geochemical Characteristics

Organic matter abundance is a critical parameter for evaluating the quality of hydrocarbon source rocks, with Total Organic Carbon (TOC, %) serving as a key indicator. TOC values are classified into five intervals: 0–0.5% (carbon-lean), 0.5–1.0% (low carbon), 1.0–2.0% (moderate carbon), 2.0–4.0% (high carbon), and >4.0% (carbon-rich).

4.1. Organic Matter Abundance

Sub-layer 7 (7 samples) exhibits TOC ranging from 0.391%–1.262% (avg. 0.574%); Sub-layer 6 (4 samples) 0.764%–0.939% (avg. 0.842%); Sub-layer 5 (4 samples) 1.005%–1.38% (avg. 1.19%); Sub-layer 4 (5 samples) 1.281%–2.19% (avg. 1.582%); Sub-layer 3 (4 samples) 1.704%–2.135% (avg. 1.702%); Sub-layer 2 (5 samples) 1.381%–2.001% (avg. 1.583%); Sub-layer 1 (4 samples) 1.047%–1.599% (avg. 1.323%). The maximum average TOC occurs in Sub-layer 3 (1.702%), while the minimum is in Sub-layer 7 (0.574%). At the sub-member scale, the D1 sub-member shows the highest average TOC (1.54%), followed by D2 (1.19%), and D3 (0.708%) (Table 3).

Table 3. TOC Statistics of Well FY10

sub-member	Sub-layer	Depth (m)	Samples (count)	TOC (%)	
				Min–Max	average
D3	7	2752.31-1768.2	7	0.391-1.262	0.574
	6	2770.89-2775.31	4	0.764-0.939	0.842
D2	5	2778.11-2782.5	4	1.005-1.38	1.190
D1	4	2784.8-2788.98	5	1.281-2.19	1.582
	3	2791.45-2796.01	4	1.704-2.135	1.702
	2	2797.65-2804.21	5	1.381-2.011	1.583
	1	2806.65-2812.01	4	1.047-1.599	1.323

Within the Dongyuemiao Member, Total Organic Carbon (TOC) values exhibit a positive correlation with increasing depth across all three sub-members:

4.2. Organic Matter Types

Kerogen maceral analysis of the studied samples indicates a composition dominated by vitrinite, humic organic matter, and inertinite, with minor sporopollen content. Vitrinite primarily exists in fragmented forms (Figure 3). The liptinite group shows the highest abundance (25%–72%, average 50%), followed by the vitrinite group (24%–66%, average 43%), while the inertinite group is least abundant (4%–15%, average 6%). Using the type index formula:

Type Index = (Lipid Group × 100 + Liptinite × 50 − Vitrinite × 75 − Inertinite × 100) / 100

The Dongyuemiao Member shale kerogen is classified predominantly as sapropelic-humic type (Type II_2) and humic type (Type III), reflecting mixed aquatic and terrestrial organic matter sources.

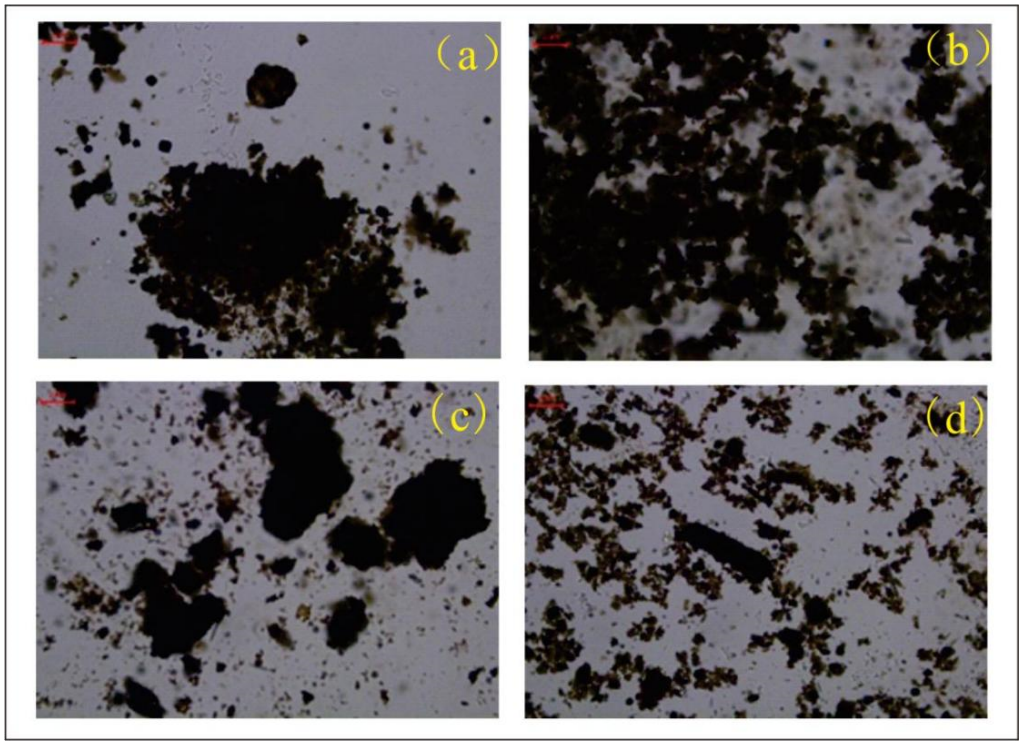


Figure 3. Photomicrographs of kerogen maceral components in the study area under microscopy

4.3. Organic Matter Maturity

Organic matter maturity, a key indicator for assessing hydrocarbon source rocks, reflects the thermal evolution of organic materials. Common evaluation methods include vitrinite reflectance (R_o), solid bitumen reflectance, rock-e pyrolysis peak temperature (T_{max}), H/C ratio, and infrared spectroscopy (IR). Given the high vitrinite content in this formation, vitrinite reflectance (R_o) is used as the primary maturity indicator. Maturity stages are defined as: immature ($R_o < 0.5\%$, biogenic gas dominant), mature ($R_o = 0.5\%–1.3\%$, liquid hydrocarbon dominant), and high-mature ($R_o = 1.3\%–2.0\%$, wet gas-condensate dominant). In the study area, the thermal evolution degree of organic-rich shale shows a positive correlation with burial depth, with R_o increasing with depth, though hydrocarbon generation stages vary across different layers and depths. Previous studies suggest that the Dongyuemiao Member shale has a vitrinite reflectance (R_o) range of 1.52%–1.58%, indicating a high-mature stage (condensate-wet gas generation) [14]. Our R_o measurements from shale samples in the Dongyuemiao Member yield a narrower range of 1.52%–1.54%, while rock-e pyrolysis Tmax values (464–494°C) confirm a mature to high-mature thermal evolution stage.

5. Shale Reservoir Pore Types

The classification of shale reservoir pores is based on the characterization of microscopic pore structures in shale cores. Scholars have categorized shale pores from multiple perspectives, including pore size, morphology, location (interparticle, intraparticle, organic-matter-hosted), genetic origin (primary or secondary), and relationships with mineral grains. Building on conventional sandstone, carbonate, and shale classification methods, Loucks et al. proposed a simplified system dividing pores into three fundamental types: interparticle pores, intraparticle pores, and organic-matter pores [9]. To comprehensively characterize the pore structure of the Dongyuemiao Member, this study integrates low-temperature nitrogen adsorption (effective for micropores <2 nm and mesopores 2–50 nm), high-pressure mercury intrusion (suitable for macropores >50 nm), and argon-ion-polished field-emission scanning electron microscopy (FE-SEM) observations. This multi-method approach ensures accurate quantification of pore size distribution and visualization of pore morphology.

5.1. Low-Temperature N_2 Adsorption Experiments and Pore Types

Adsorption isotherms serve as foundational data for studying adsorption phenomena on solid surfaces and within pores, enabling the quantification of pore-related parameters such as specific surface area and pore size distribution. According to the IUPAC classification, five types of adsorption isotherms exist (Figure 4.), each reflecting distinct pore sizes, quantities, and structural characteristics. The shapes of adsorption isotherms and their associated hysteresis loops provide critical insights into pore types [15]. Hysteresis loops are categorized into four types (H1–H4) under the IUPAC framework to characterize different pore structures (Figure 4.). H1 and H2 hysteresis loops exhibit a distinct plateau in the high-pressure region of the isotherm, indicating uniform pore size distribution, while H3 and H4 loops lack such plateaus, reflecting complex and heterogeneous pore networks. Specifically, H1 corresponds to cylindrical pores, H2 to ink-bottle-shaped pores, H3 to slit-shaped pores formed by aggregated plate-like particles, and H4 to parallel-plate pores with narrow slits [16]. These classifications align with SEM-observed pore geometries and fractal modeling results, confirming the dominance of mesopores (2–50 nm) and macropores (>50 nm) in the Dongyuemiao shale.

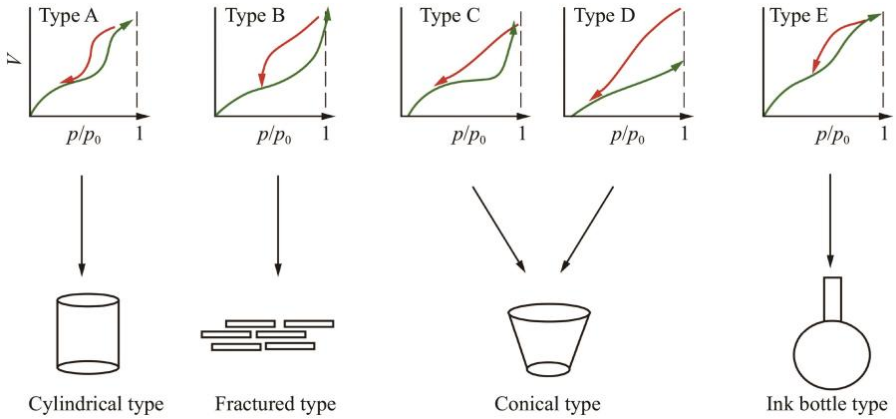


Figure 4. Schematic diagram of hysteresis loops and corresponding pore geometries (IUPAC classification)

The low-temperature N_2 adsorption-desorption curves of the experimental samples exhibit Type IV isotherms with H4-type hysteresis loops (Figure 5). When the relative pressure (P/P_0) is below 0.9, the adsorption curve shows a gradual and steady increase in adsorption volume, while a rapid rise occurs as P/P_0 exceeds 0.9, culminating in maximum adsorption near $P/P_0 \approx 1$. The desorption curve demonstrates a slow decline in the P/P_0 range of 0.9–0.6, followed by an abrupt stepped drop at $P/P_0 \approx 0.5$, forming a pronounced hysteresis loop with an open slit-like morphology. This H4 hysteresis behavior reflects complex pore structures dominated by parallel-plate geometries, consistent with SEM observations of slit-shaped pores in clay-organic aggregates. All samples display Type IV isotherms and H4 hysteresis loops, confirming the prevalence of narrow, layered pore networks in the Dongyuemiao shale.

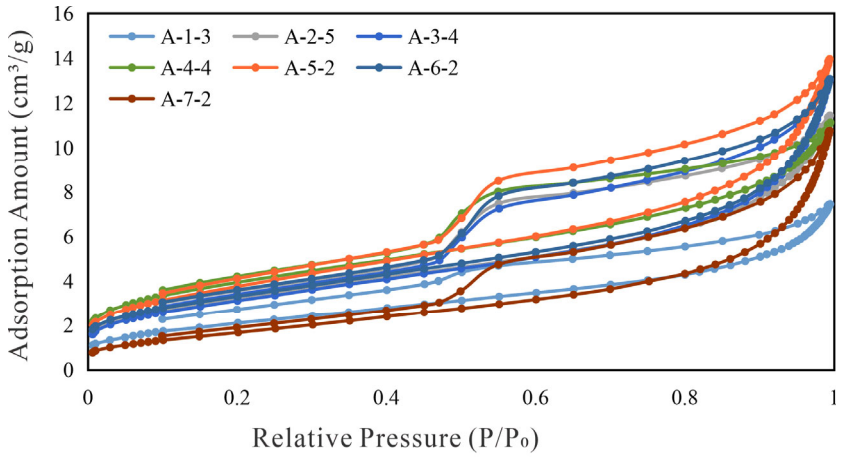


Figure 5. N_2 adsorption-desorption isotherms

The N_2 adsorption-desorption isotherms of samples A-2-5, A-3-4, A-4-4, A-5-2, and A-6-2 exhibit nearly identical behavior, with comparable adsorption capacities. In contrast, samples A-1-3 and A-7-2 display significantly lower adsorption capacities than the other five samples. Among all seven samples, A-5-2 achieves the highest adsorption capacity of 13.85 cm³/g at near-saturation relative pressure ($P/P_0 \approx 1$), while A-1-3 shows the lowest adsorption capacity of 7.38 cm³/g.

5.2. Shale Reservoir Pore Size Distribution

The pore classification system commonly used in China categorizes shale pores into three types based on pore size: microporous (diameter <2 nm), mesoporous (2–50 nm), and macroporous (>50 nm) [15–16]. Low-temperature N_2 adsorption experiments indicate that the tested samples primarily exhibit pores within the 1–30 nm range (pores <1 nm were not characterized), with dominant development of micropores and mesopores. Sample A-2-5 shows a partial concentration of pores around 60 nm (Figure 6), suggesting a bimodal distribution with peaks in the micro-mesopore (1–30 nm) and macropore (>50 nm) ranges.

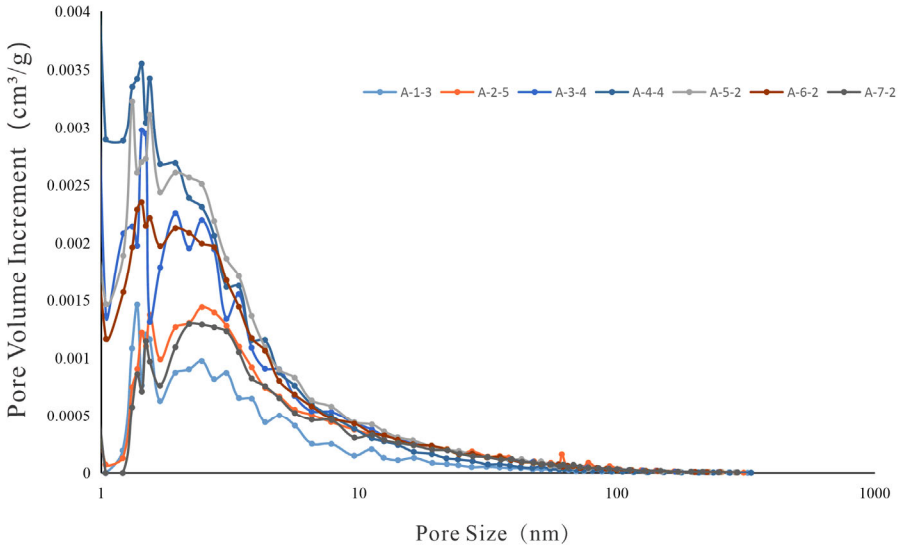


Figure 6. Relationship between pore size and pore volume increment

Analysis of mercury intrusion capillary pressure (MICP) curves shows that mercury intrusion volume increases with rising capillary pressure, exhibiting two distinct stages: an initial rapid rise followed by a gradual plateau. A notable inflection point occurs at pressures exceeding ~100 MPa, where the curve stabilizes (Figure 7). The seven samples are categorized into two groups based on displacement pressures: Group 1 (A-1-2, A-2-4, A-3-5, A-4-3) with displacement pressures around 30 MPa, and Group 2 (A-5-2, A-6-1, A-7-2) with significantly higher displacement pressures (~50 MPa). Prior to reaching displacement pressure, Group 1 samples exhibit greater mercury intrusion volumes than Group 2, indicating coarser pore-throat systems in the former. Minor surges in mercury intrusion at 0.2 MPa (A-1-2) and 0.7 MPa (A-2-4) suggest the presence of micro-fractures. All samples demonstrate similar mercury withdrawal efficiencies (~40%), reflecting comparable pore connectivity. These results align with HPMI data and pore-throat size distributions, confirming the dominance of mesopores (2–50 nm) and slit-shaped geometries in the Dongyuemiao shale.

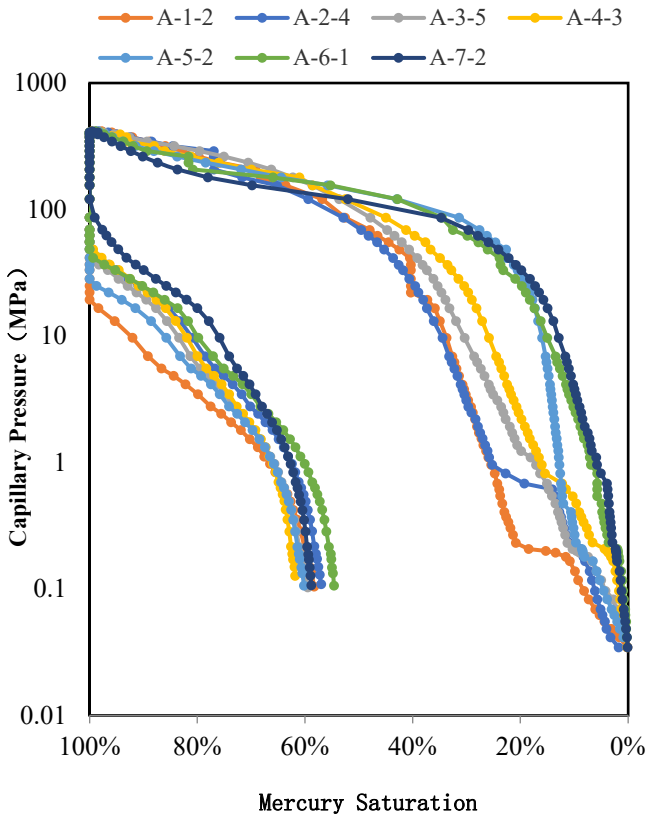


Figure 7. Mercury intrusion capillary pressure (MICP) curves

6. Influencing Factors of Shale Reservoir Pore Structure

6.1. Mineral Composition

The Dongyuemiao Member shale, characterized by high clay mineral and quartz content, demonstrates distinct mineralogical controls on pore structure. Clay minerals significantly influence pore volume, with variations across lithofacies. In clay-rich shale lithofacies, increased clay content positively correlates with micropore, mesopore, and macropore volumes. In contrast, silty shale lithofacies exhibit weak or negative correlations between clay content and pore metrics. Quartz content impacts pore structure differently: in silty shale, quartz enhances pore volume and specific surface area by preserving primary pores and forming interparticle pores due to its compressive resistance, while in clay-rich shale, quartz shows negative correlations with pore volume and surface area, likely due to pore-filling by authigenic quartz cement. These trends align with SEM-observed pore geometries and fractal dimensions, confirming mineralogical control on pore heterogeneity.

6.2. Lithofacies

The study area comprises five lithofacies: carbon-bearing silty shale, low-carbon silty shale, medium-carbon silty shale, medium-carbon clay-rich shale, and high-carbon clay-rich shale. Across these lithofacies, the average micropore volume remains relatively consistent (~0.002 cm^3/g), while mesopore volume varies significantly—peaking in low-carbon silty shale (>0.012 cm^3/g) and reaching a minimum in medium-carbon silty shale (<0.01 cm^3/g). Macropore volume is notably low in medium-carbon silty and clay-rich shales (<0.004 cm^3/g), whereas other lithofacies exceed this threshold. Micropores contribute less than 10% of the total pore volume across all lithofacies, mesopores dominate with ~65% contribution, and macropores account for ~25%, highlighting mesopores as the primary pore type governing storage and flow capacity.

6.3. Organic Carbon Content

The total organic carbon (TOC) content in the Dongyuemiao Member shale varies stratigraphically, with the highest values observed in Sub-members 1–4 of the Dong-1 Member, where some samples exceed 2%. In Sub-member 5 of the Dong-2 Member, TOC averages around 1%, while samples from Sub-members 6–7 of the Dong-3 Member predominantly have TOC below 1%. The influence of TOC on pore volume differs across lithofacies: clay-rich shale lithofacies show a positive correlation between TOC and pore volume, likely due to enhanced development of organic-hosted pores, whereas silty shale lithofacies exhibit a weak negative correlation. These trends suggest that higher TOC in clay-rich shales promotes organic pore formation, contributing to mesopore-dominated pore systems, while quartz-dominated silty shales experience pore volume reduction with increasing TOC, possibly due to mineralogical constraints on pore preservation.

7. Summary

1. Mineral Composition

The Dongyuemiao Member shale reservoir is primarily composed of clay minerals, followed by quartz. The clay mineral assemblage is dominated by illite, with subordinate chlorite and kaolinite. The lithofacies in this member are predominantly clay-rich shale and silty shale.

2. Organic Carbon Content (TOC) and Thermal Maturity

The average TOC values vary stratigraphically: the Dong-

1 Sub-member has the highest TOC (1.54%), followed by Dong-2 (1.19%), and Dong-3 (0.708%), all within the medium-carbon range. Kerogen types are mainly sapropelic-humic (Type II_2) and humic (Type III). Vitrinite reflectance (R_0) ranges from 1.52% to 1.54%, indicating high thermal maturity.

3. Pore Characteristics

The low-temperature N_2 adsorption-desorption isotherms of the Dongyuemiao shale are classified as Type IV with H4 hysteresis loops, consistent with slit-shaped and plate-like pore geometries observed via SEM. Pore sizes are predominantly distributed in the 2–100 nm range.

4. Lithofacies-Specific Controls on Pore Volume

In clay-rich shale lithofacies, increased clay mineral content positively correlates with pore volume. In contrast, silty shale lithofacies show no significant correlation. Quartz enhances pore volume in silty shales but reduces it in clay-rich shales due to pore-filling cementation. Higher TOC promotes pore volume in clay-rich shales (likely through organic pore development) but exhibits a weak negative correlation in silty shales.

References

[1] Zou Caineng, Dong Dazhong, Wang Yuman, et al. Shale gas characteristics, challenges, and prospects in China (Part I) [J]. Petroleum Exploration and Development, 2015, vol. 42, no. 6, pp. 689–701.

[2] Ma Xinhua, Xie Jun, Yong Rui, et al. Geological characteristics and high-yield controlling factors of shale gas reservoirs in the Longmaxi Formation, southern Sichuan Basin [J]. Petroleum Exploration and Development, 2020, vol. 47, no. 5, pp. 841–855.

[3] Jin Zhijun, Hu Zongquan, Gao Bo, et al. Controlling factors of shale gas enrichment and high production in the Wufeng-Longmaxi formations, southeastern Sichuan Basin [J]. Earth Science Frontiers, 2016, vol. 23, no. 1, pp. 1–10.

[4] Guo Xusheng, Hu Dongfeng, Wei Zhihong, et al. Discovery and exploration insights of the Fuling shale gas field [J]. China Petroleum Exploration, 2016, vol. 21, no. 3, pp. 24–37.

[5] Jiang Tao, Jin Zhijun, Liu Guangxiang, et al. Investigating the pore structure characteristics and reservoir capacities of Lower Jurassic continental shale reservoirs in the northeastern Sichuan Basin, China [J]. Frontiers in Earth Science, 2022, vol. 10, 886907. DOI: 10.3389/feart.2022.886907.

[6] Zou Caineng, Zhang Guangya, Tao Shizhen, et al. Geological features, major discoveries, and unconventional petroleum geology in global oil and gas exploration domains [J]. Petroleum Exploration and Development, 2010, vol. 37, no. 2, pp. 129–145.

[7] Hu Degao, Shu Zhiguo, Guo Zhanfeng, et al. Discovery of the first shale condensate reservoir in the Jurassic Fuyou-10HF well, Fuxing area, eastern Sichuan [J]. Geology in China, 2021, vol. 48, no. 6, pp. 1980–1981.

[8] Liu Wei. Formation mechanisms and evolution of sedimentary basins: A case study of the Sichuan Basin [J]. China Petroleum and Petrochemical, 2016, no. 21, pp. 17–18.

[9] Shu Zhiguo, Zhou Lin, Li Xiong, et al. Geological characteristics and exploration prospects of continental shale condensate reservoirs in the Dongyuemiao Member of the Jurassic Ziliujing Formation, Fuxing area, eastern Sichuan Basin [J]. Oil & Gas Geology, 2021, vol. 42, no. 1, pp. 212–223.

[10] Zou Yutao, Duan Jinbao, Zhao Yanjun, et al. Structural characteristics and evolution of the high-steep fault-fold belt in eastern Sichuan [J]. Acta Geologica Sinica, 2015, vol. 89, no. 11, pp. 2046–2052.

[11] Sun Shasha, Dong Dazhong, Li Yucong, et al. Geological characteristics and controlling factors of hydrocarbon accumulation in the Da'anzhai Member of the Jurassic Ziliujing Formation, Sichuan Basin [J]. Oil & Gas Geology, 2021, vol. 42, no. 1, pp. 124–135.

[12] Jiang Wenjian, Hou Mingcai, Ma Hualing, et al. Sedimentary facies of the Lower Jurassic Zhenzhuchong Member in the Jiulongshan area, northwestern Sichuan [J]. Journal of Geomechanics, 2014, vol. 20, no. 1, pp. 48–60.

[13] Liu Zhongbao, Liu Guangxiang, Hu Zongquan, et al. Lithofacies types, associations, and their implications for shale oil and gas exploration: A case study of the Middle-Lower Jurassic in the Sichuan Basin [J]. Natural Gas Industry, 2019, vol. 39, no. 12, pp. 10–21.

[14] Li Shilin, Zhang Wenji, Li Yanjun, et al. Evaluation of source rocks in the Dongyuemiao Member of the Lower Jurassic Ziliujing Formation, eastern Sichuan [J]. Natural Gas Exploration and Development, 2021, vol. 44, no. 2, pp. 11–18.

[15] Loucks R G, Reed R M, Ruppel S C, et al. Morphology, genesis, and distribution of nanometer-scale pores in siliceous mudstones of the Mississippian Barnett Shale [J]. Journal of Sedimentary Research, 2009, vol. 79, no. 12, pp. 848–861.

[16] Xia Dong, Yang Zhi, Gao Tian, et al. Characteristics of micro- and nano-pores in shale oil reservoirs [J]. Journal of Petroleum Exploration and Production Technology, 2020, vol. 10, pp. 1–13.